SABRE: The Silicon Array for Branching Ratio Experiments

E.C. Good[a,1], B. Sudarsan[a], K.T. Macon[a], C.M. Deibel[a], L.T. Baby[b], J.C. Blackmon[a], C. Benetti[b], J.C. Esparza[b], N. Gerken[b], K. Hanselman[b], G.W. McCann[b], A.B. Morelock[b], J.F. Perello[b], K.H. Pham[a], E. Rubino[b], E. Temanson[b], I. Wiedenhöver[b]

[a] *Department of Physics & Astronomy, Louisiana State University, Baton Rouge, LA 70803*
[b] *Department of Physics, Florida State University, Tallahassee, FL 32306*

Abstract

The Silicon Array for Branching Ratio Experiments (SABRE) has been developed for use to study reactions of interest to nuclear structure and astrophysics. The array has been incorporated into the Super Enge Split-Pole Spectrograph (SE-SPS) experimental setup at Florida State University's John D. Fox accelerator laboratory to detect charged-particle decays in coincidence with reaction products detected by the SE-SPS focal plane detector. Its construction and electronics processing are discussed, as well as the commissioning data used to validate its performance.

Keywords: Silicon detector, Enge split-pole spectrograph, charged particle coincidence, digital electronics

1. Introduction

The Super Enge Split-Pole Spectrograph (SE-SPS) [1] is a versatile experimental instrument that can be used for a variety of stable beam measurements important for nuclear astrophysics and structure. For example, Refs. [2, 3, 4] describe measurements of energy levels in resonant nuclei and branching ratios

Email address: erincgood@gmail.com (E.C. Good)
[1] Current address: Facility for Rare Isotope Beams, 640 S. Shaw Ln, East Lansing, MI 48824

important for astrophysical calculations, while Refs. [5, 6] describe measurements of spectroscopic factors and level schemes pertaining to nuclear structure.

The John D. Fox Accelerator laboratory at Florida State University (FSU) recently acquired the Enge Split-Pole Spectrograph formerly housed at Yale University's Wright Nuclear Structure Laboratory (WNSL). The setup was dismantled in 2013 after the cessation of operations at the WNSL and was transported to FSU for installation. In addition, upgrades were made to the auxiliary detector systems. Construction of the support pedestal for the SE-SPS, which supports the entire 34-ton structure, began in Fall 2015. The magnet itself was placed in January 2017, with gas-handling and power systems being installed in the first half of 2017. Fall of 2017 marked the installation of the target chamber, followed by construction of a new beamline with the first beam on target achieved in June 2018.

The SE-SPS has a radius of curvature ranging from 51 to 92 cm, a dispersion $D = \Delta x/\Delta\rho$ of 1.96, and a maximum acceptance of 12.8 msr, the largest of any Enge SPS ever built. The dispersion and focusing optics of the magnet were calculated to achieve uniform dispersion and a straight focal plane; the details of this design feature are described in detail in Ref. [7]. The spectrograph's complementary detector systems include a gas-filled focal plane detector backed by a scintillator bar acquired from the WNSL [8]; the focal plane detector has been refurbished and placed at the focal plane of the SE-SPS to detect light, charged reaction products. A silicon detector array, the Yale Lamp Shade Array (YLSA) [9], was also acquired. However, given the advances in Si detector design and digital electronics, the Silicon Array for Branching Ratio Experiments (SABRE) was developed to replace YLSA. The CAKE (Coincidence Array for K600 Experiments), implemented with the K600 cyclotron and QDD magnetic spectrometer at iThemba Labs, Cape Town, South Africa [10], also has a similar configuration to YLSA, but both the CAKE and SABRE use a different Si detector design as discussed below. Additionally, the power of SABRE lies in its ability to achieve lower energy thresholds and higher throughputs than previous silicon arrays with its digital electronics, which are discussed below.

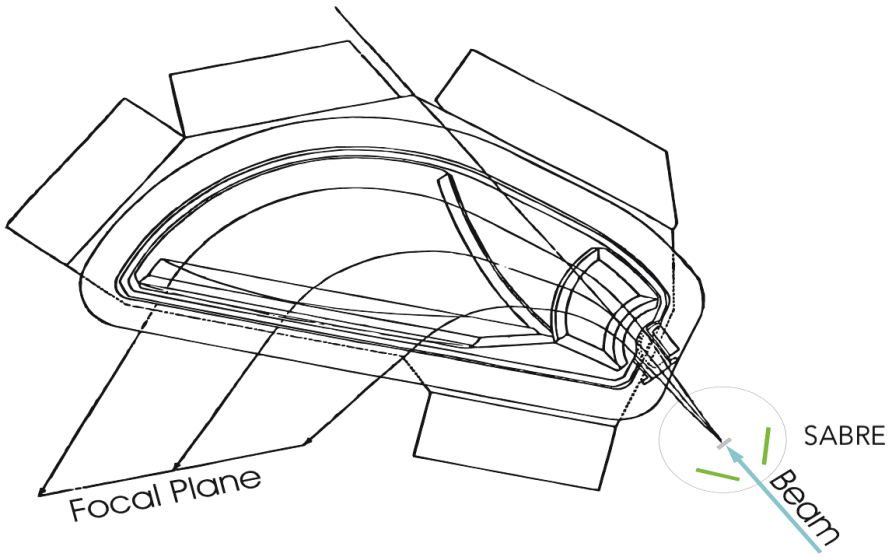

Figure 1: A schematic of the SE-SPS setup, adapted from [9]. The beam (blue) enters the target chamber (grey circle) through an aperture in the SABRE mount. Light reaction byproducts continue along the curved trajectory lines through the SE-SPS and into the focal plane detector (not shown). In the target chamber, charged-particle decays from the excited states populated in the target are detected at backward angles by SABRE (green).

The setup of the spectrograph's current auxiliary detectors is shown in Fig. 1. Typically, transfer or charge-exchange reactions are performed using stable, light-ion beams that impinge on a heavy target and populate excited states in the product nuclei, which remain in the target. The light-reaction byproducts continue through the target and are momentum analyzed by the SE-SPS before being detected in the focal plane detector. Charged-particle decays from the excited nuclei in the target are then detected by SABRE, placed at backward angles to the target. The combination of these two detector systems allows the measurement of the excited states populated in the heavy product via the reaction and charged-particle decays that the excited state undergoes.

The focal plane detector consists of a rectangular proportional counter filled with isobutane and backed by a plastic scintillator, described in detail in Ref.

[8]. In the gas-filled section, particle positions can be determined from two sets of pickup pads read out by delay lines positioned above the two sets of anode wires; two sets of position information (front and rear hereafter) allow for the reconstruction of particle trajectories within the detector in post-processing. Additionally, several different energy loss signals can be read out from the proportional counter: from the anode wires, the cathode plate, and even the delay-line energy signals. The plastic scintillator then stops the particles from the proportional counter and measures their residual energy. In total, the focal-plane detector gives two position signals, a variety of energy loss signals, and a residual energy signal from the scintillator, as well as timing information from each of these signals.

The design of SABRE is described in Section 2 while its digital electronics and data acquisition systems are described in Section 3. Section 4 then discusses the commissioning run used to verify SABRE's performance, with a brief explanation of data analysis techniques.

2. SABRE Design

SABRE is a backward-angle silicon detector array that can be used for coincidence measurements with the SE-SPS. Figure 2 shows the geometry of the array in relation to the beam and target position in the target chamber of the SE-SPS with a photograph of the array on the bench. The array consists of five Si detector segments, discussed below, oriented in a lampshade configuration. The lampshade design allows for maximal angular coverage, covering θ_{lab} angles from approximately 105° to 165°. The distance from the base of the mount to the target ladder is 124.5 mm, and the detectors themselves are at a 50° angle from the beam axis. Details of the geometric efficiencies are discussed in the sections below.

The array consists of five Micron Semiconductor, Ltd. MMM model detectors. The MMM detectors consist of 16 junction-side annular strips and eight ohmic-side radial strips. SABRE can be equipped with either of two sets of

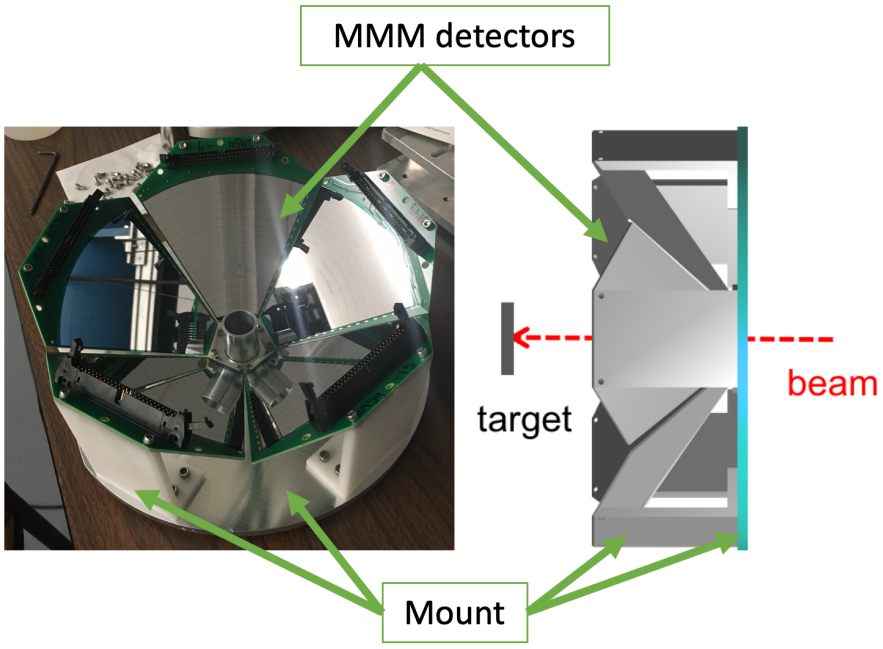

Figure 2: A photograph of SABRE with all detectors installed on the bench, left, and a CAD drawing of SABRE, right. The right side shows a side-on view with the target and beam positions labeled. MMM detectors and the mount pieces are labeled by the green arrows in both the CAD drawing and photograph.

	Set A	Set B
Detector thickness	400 μm	500 μm
Deadlayer thickness	500 nm	50 nm
Minimum proton energy threshold in deadlayer	90 keV	10 keV
Depletion voltage on junction side	-60 V	-60 V
Initial leakage current range	0.11-0.38 μA	0.23-0.54 μA

Table 1: Various characteristics of each set of MMM Si detectors used in SABRE.

five MMM detectors: one set has a quoted thickness of 400 μm and a 500 nm deadlayer, and the second set has a quoted thickness of 500 μm and a 50 nm deadlayer. Specific characteristics of each detector set can be seen in Table 1. Deadlayer thicknesses were verified in the lab to be within 40% of quoted values by comparing the energy loss of alpha particles from a ^{241}Am source at different relative angles through the deadlayer. This equates to a minimum proton energy threshold of 90 keV and 10 keV to penetrate the thick and thin dead layers, respectively. The thin deadlayer detectors should thus allow for measurements of lower energy particle decays. The segmentation of the detectors into annular and radial strips allows for analysis of decays in both theta and phi, respectively.

Additionally, several measures were taken to shield the array from beam scattering and electrons created in the target and beamstop. Several of these were implemented in the YLSA array and described in Ref. [11], such as biasing the target ladder at +600 V, biasing the SABRE mount at +500V, and implementing a physical shield just downstream of the target ladder consisting of 0.25" thick aluminum to protect the array from beamstop backscattering. Each target on the target ladder has a rare earth magnet placed above and below it for electron suppression. Another protective measure taken was to bias the junction sides of the detectors with negative voltage (-60V) as opposed to biasing the ohmic sides with positive voltage. While producing the same depletion effect in the detectors, this provides additional electron suppression.

A significant advantage of the newly designed SABRE array is its increased

angular coverage compared to YLSA, by roughly a factor of two. To determine the geometric efficiency, the array was modeled using a Monte Carlo simulation [9], and known branching ratios were measured to benchmark the simulations as discussed below. The Monte Carlo simulation calculates that the array has a geometric efficiency of roughly 30% for an isotropic particle decay, though this varies depending on the reaction and properties of the decaying state as discussed in detail below.

3. Electronics

While YLSA used conventional (analogue) electronics, a completely digital system has been implemented for SABRE and the focal plane detector. The advantages of using digital electronics include lower dead times, larger dynamic range, and lower thresholds [12]; however, lower thresholds require the utilization of an external trigger and a specific set of digitizer parameters, which are described in detail below. Because digital electronics are utilized for pulse processing both the focal plane detector and SABRE signals, the synchronization of timestamps across both SABRE and focal plane detector digitizer modules is straightforward.

3.1. Focal Plane Detector

All focal plane signals are processed on a single CAEN v1730 digitizer board using CAEN's proprietary Pulse Shape Discrimination (DPP-PSD) firmware. This firmware implements digital charge integration within fixed gate intervals set by the user and a digital constant-fraction discriminator that creates a trigger for the gates and a timestamp for the signal. While the firmware allows for pulse-shape discrimination through the use of both a short and long time integration gate, only the long gates were used in this application. The long gate is set such that it charge-integrates the entire pulse, which is proportional to the total energy collected, and is used here to process the ΔE outputs of the focal plane detector and the residual energy deposited in the scintillator.

Because the firmware allows for signal integration with varying time constants, smoothing factors, and other parameters unique to each channel, the same module could be used for all signal types in the focal plane detector, from the short scintillator pulses to the relatively slow cathode plate pulses. More details on all the functions of the DPP-PSD firmware and how to set specific parameters can be found in Ref. [13], as firmware parameters for each signal vary for every experiment. We verified that the focal plane position resolution (found by reading out the timing signals on each end of the delay lines) was equivalent to the resolution obtained with analogue electronics, while the energy resolution (relevant for particle identification) was improved.

3.2. SABRE

The SABRE signals exit the target chamber via printed-circuit-board (PCB) feedthroughs and are first processed by preamplifier systems, with one preamplifier chip per channel, initially developed for the LASSA array [14]. The preamplifiers are charge-sensitive with resistive feedback that shape and amplify the signals with a sensitivity of 27 mV/MeV and are supported by custom 36-channel PCB motherboards that also provide bias voltage to the silicon detectors in the array. The preamplifier output signals are fed through ribbon cables to Mesytec MDU-16 modules, which convert the signals to a unipolar lemo output (preparing them for the individual channel MCX input to the digitizers) and apply an adjustable gain common to all channels in each module [15].

The resulting unipolar signals are then fed to CAEN 1730 and 1725 digitizers utilizing CAEN's proprietary Pulse Height Analysis (DPP-PHA) firmware. DPP-PHA firmware uses a trapezoidal filtering algorithm designed for extracting pulse heights from resistive-feedback, charge-sensitive preamplifiers to create a trapezoid from the signal; the height of the trapezoid produced is proportional to the energy deposited in the detector [16]. The detector resolution and count rate stability were optimized by altering the different trapezoidal parameters in the firmware (these parameters will vary depending on the characteristics

of the detectors and preamplifiers used). An event in the DPP-PHA firmware is comprised of channel and digitizer-board numbers, energy, and timestamp information.

3.3. External Triggering and Digitizer Setup

For all SABRE experiments thus far, the data acquisition system used CAEN's CoMPASS software, both for the initialization of the digitizer firmware parameters and the readout and recording of data from the individual digitizer modules. Eventbuilding, or the grouping of different detector signals from the same reaction event, is done offline using each channel's recorded timestamp. Work is ongoing to make the setup NSCLDAQ (the National Superconducting Cyclotron Laboratory's Data Acquisition System) compatible.

In order to have a common internal clock reference between all digitizer modules, the clock signal in the first board is propagated to all other boards and synchronized via short twisted-wire cables terminated by AMPMODU connectors (i.e. clock cables). In addition, the run start/stop signals are also propagated along the digitizer chain via LEMO cables so that the timestamps in each board are set to zero synchronously at the start of each run. This is done by cabling the "TRG OUT" lemo port on the first digitizer to the "SYNC IN" lemo port on the next; this continues down the chain of digitizers being used to the last board (more detailed information on correctly implementing the digitizer daisy chain setup and the synchronization process can be found in Ref. [17]). This acquisition mode is called the "TRG OUT-SYNC IN" mode and must be selected in CoMPASS to synchronize the clocks. The proper cabling scheme for this setup can be seen in Fig. 3, indicated via the green arrows. This running mode also requires an external start signal (NIM or TTL) to start data acquisition into the first, or parent, board, which must be applied before starting a run in CoMPASS; this was implemented with a Lecroy 222 NIM Dual Gate and Delay Generator module and can be seen in Fig. 3 indicated by the blue arrow.

The digitizer used for the focal plane detector runs in a self-triggering, or

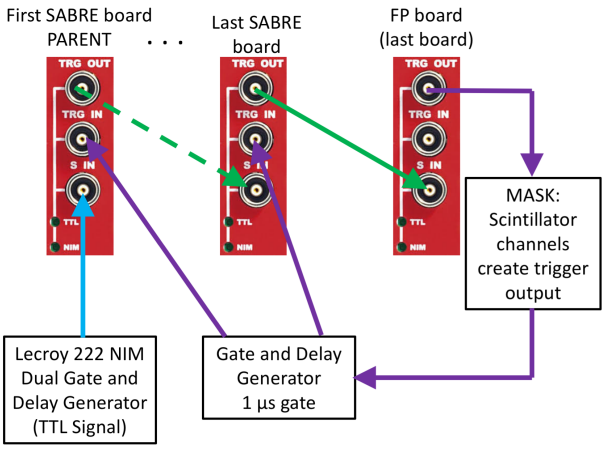

Figure 3: Digitizer cabling scheme for the setup described in the text, with the first and last SABRE digitizer boards represented (other boards are inserted where the ellipses are and are cabled similarly) and the focal plane (FP) board being the last in the chain. The green arrows indicate the cabling scheme required to synchronize the run start/stop signal. The blue arrow indicates the input of the external TTL start signal required to start a run in the software. The purple arrows indicate the propagation the external trigger to all the SABRE boards in the setup. Note that the focal plane detector board is last in the chain so that its "TRG OUT" signal can be used for the external triggering. More details in the text.

"global OR" triggering mode, which must be selected in CoMPASS. With this scheme, all focal-plane signals are recorded whether or not they are coincident with events in SABRE. This digitizer must be placed last in the digitizer chain for the triggering scheme described here.

When running CoMPASS version 1.3.0, data can be successfully recorded with low thresholds. However, this results in high data rates (∼1 kHz per channel) due to the low-energy events of interest coinciding with uncorrelated background events such as beam scattering and electronic noise. An external trigger reduces the recorded data rate to a manageable level. Successfully collecting SABRE events of interest at low detection thresholds thus requires the implementation of an external trigger from the focal plane detector to minimize the recording of uncorrelated signals in SABRE on the firmware of each SABRE board (e.g. scattering and noise) while keeping the coincidences of interest. Note that CoMPASS version 1.3.0 or higher is required to utilize the external triggering scheme described below.

To implement an external trigger for signal recording in SABRE digitizers, the boards are set to a "TRG IN level gate" triggering mode in CoMPASS requiring a level sensitive TTL or NIM signal on the "TRG IN" lemo port of that board to validate a SABRE trigger. If there is no external gate signal, no data is recorded. Additionally, the "Coincidence Window" parameter in CoMPASS is set to 496 ns to create a "TRG_REQ" (trigger request) signal on each SABRE board. The "TRG_REQ" time is the length of time a SABRE board will wait for validation from the external trigger; if the board does not receive an external trigger validation within this timeframe, the signal is not recorded. The specific locations of these parameters in the CoMPASS software are described in Ref. [18].

The external trigger for the SABRE digitizers was generated from the focal plane scintillator signals using the "mask" feature written into a "FreeWrites" file that CoMPASS applies to the firmware of each board. This particular mask generated a trigger output from the focal plane board's "TRG OUT" port created from just the scintillator channels' signals that was shaped into a 1 μs-long

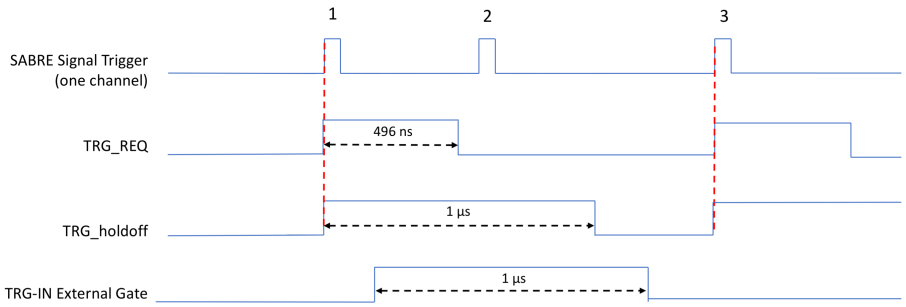

Figure 4: Three SABRE signal triggers are shown for one channel (top), with the trigger request (middle top), trigger holdoff (middle bottom), and the external gate (bottom). Signal 1 is recorded as the external gate falls within the trigger request time of the board; a trigger holdoff is also applied. Signal 2 does not get recorded even though it is within the external gate because it occurs during the trigger holdoff for signal 1. Signal 3 does not get recorded due to its trigger request not being validated by an external gate.

logic pulse (using a Phillips 794 Quad Gate/Delay Generator), which was fanned out into each SABRE board. Figure 3 shows the setup and correct propagation of this signal, while Fig. 4 demonstrates how the external gate is used to validate event recording on the SABRE boards. The "Coincidence Window," or "TRG_REQ," time of 496 ns allows for the validation of SABRE events by light reaction particles even though they must travel through the spectrograph first. The time-of-flight of reaction particles through the spectrograph is on the order of a few 100 ns, such that the external gate signal still arrives in time for validating the SABRE signals.

In conjunction with the external trigger gate, all SABRE channels had a trigger holdoff of 1 μs applied (i.e. length of time required before the data acquisition will accept another event trigger) in order to prevent multiple triggering within one external trigger validation window [19]; this length is equal to double the length of the "Coincidence Window" (i.e. "TRG_REQ") parameter to avoid double coincidences as described in Ref. [19]. Figure 4 shows how this holdoff works in relation to multiple SABRE events on a single channel.

When paired with a pileup rejection algorithm in the SABRE boards' firmware, this scheme allowed the boards to reliably process raw trigger rates of up to 10 kHz per SABRE channel while recording only gated events of interest. This allows for significantly lower thresholds in the silicon detectors compared with analogue electronics while producing data files of a manageable size.

Note that the threshold of each channel in each board can be adjusted accordingly via CoMPASS to modify raw rates; different beam on target combinations will have higher or lower raw trigger rates (mostly dependent on target Z, thickness, and beam current).

4. Commissioning

To test the capabilities of the fully digitized SABRE system and to ascertain the geometric efficiency, an experiment to measure known α-particle branching ratios of states in ^{16}O via $^{19}\mathrm{F}(p,\alpha)^{16}\mathrm{O}^{*}(\alpha)^{12}\mathrm{C}$ was performed at the John D. Fox Accelerator Laboratory at FSU. A beam of 10-MeV protons bombarded a 100-μg/cm^2 LiF target on a 20-μg/cm^2 carbon backing. The magnetic field was set to 5.8 kG, the SPS was set at a 15° angle relative to the beam, and the aperture of the SPS was open to an acceptance of $\pm$30.2 mrad in the horizontal direction and full acceptance ($\pm$80 mrad) in the vertical direction. Note that all digitizers were run in the self-triggering scheme (recording all incoming signals above threshold), as opposed to the scheme described above, for this experiment as low thresholds were not required in the SABRE digitizers. The α particles detected in the gas-filled focal plane detector were used to identify states of interest populated in ^{16}O. Alpha decays from the excited states populated in ^{16}O were detected in the SABRE array in coincidence with these particles in order to measure branching ratios.

Alpha-particle reaction products associated with states of interest in ^{16}O are identified in the focal plane detector through their characteristic energy loss, as shown in Fig. 5. By selecting the alpha-particle group, a spectrum of excited states populated in ^{16}O can be produced (Fig. 6). The peak areas determine

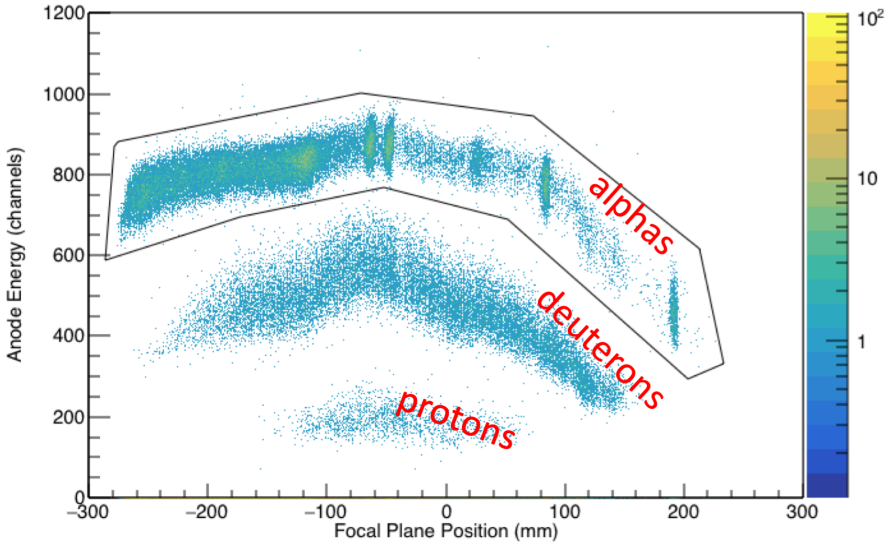

Figure 5: Focal plane position versus anode wire energy. The particle groups shown here are alphas, deuterons, and protons, as labeled. A gate is drawn around the alpha particles.

the number of events accepted by the SPS associated with the population of each state of interest.

The position of these alpha particles along the focal plane is plotted versus the energy deposited in SABRE by the α-decay particles from ^{16}O, and a gate is placed around the diagonal line corresponding to the alpha-decays to the ground state of ^{12}C (Fig. 7). These counts can then be projected onto the focal plane position axis as shown in Fig. 8. By comparing the number of counts in the peaks of interest in Figs. 6 and 8 and folding in the geometric efficiency, a value for the branching ratio can be extracted.

Here, states in ^{16}O with 100% alpha-particle branching ratios have been measured to verify the accuracy of the Monte Carlo simulation and benchmark the performance of SABRE. The simulation, adapted from [9], reproduces the reaction of interest and its decay (with appropriate l transfer) into a mockup of SABRE, and allows for a calculation of geometric efficiency. The output also

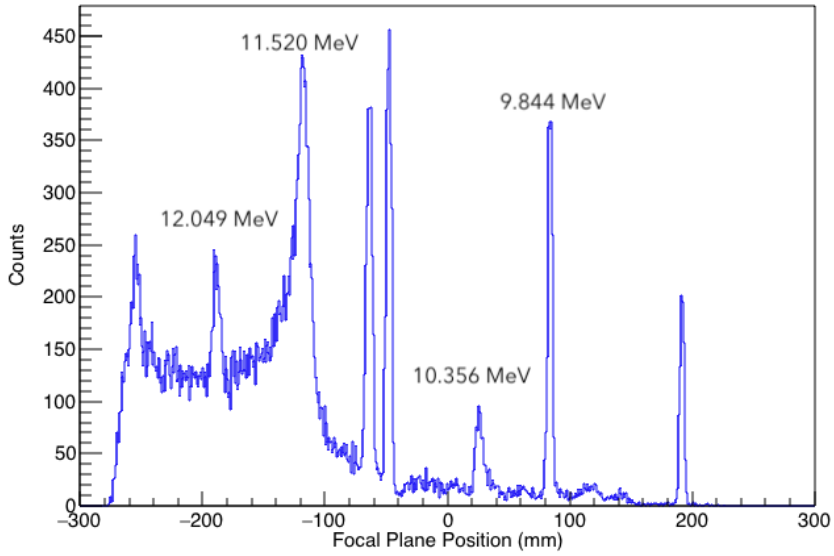

Figure 6: A projection of the gated alpha particles in the focal plane (see Fig. 5). States of interest with 100% proton branching ratios in ^{16}O are labeled by excitation energy.

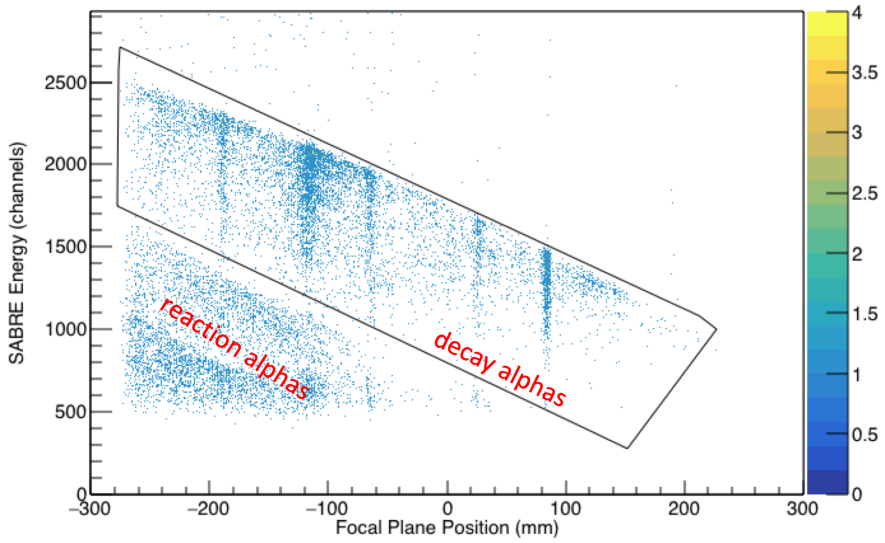

Figure 7: Focal plane position versus energy deposited in SABRE. The gate is drawn around alpha-particle decays to the ground state of ^{12}C from excited states populated in ^{16}O, as labeled. Other diagonal lines represent alphas from the initial $^{19}\mathrm{F}(p,\alpha)^{16}\mathrm{O}$ reaction that are emitted at backward angles.

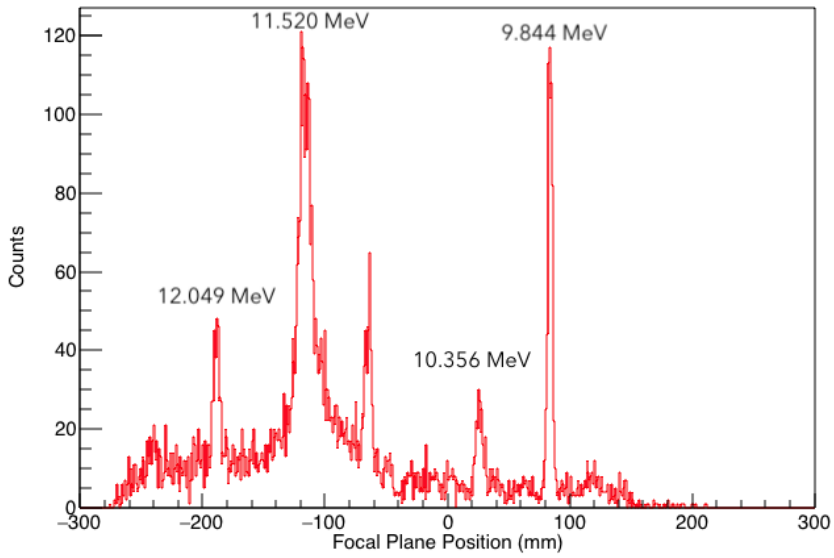

Figure 8: Focal plane position of alpha-particle reaction products associated with states in ^{16}O gated on α-particle decays to the $^{12}C_{g.s.}$ measured in SABRE. States of interest with 100% alpha-particle branching ratios in ^{16}O are labeled by their energy.

allows for the efficiencies of individual strips to be determined. The simulation for this experiment was run for one million events per state of interest and the errors combine statistical uncertainties and the uncertainty in measured mount dimensions (e.g. the mount distance from the target ladder and the angles of the detectors, as these allow for variable mounting dimensions). The values of the SABRE measurements and the Monte Carlo simulation findings are shown in Table 2.

	Geometric Efficiencies of 100% Branching Ratios	
Excitation Energy	Calculated	Measured
9.844 MeV	27.2(32) %	31.5(14) %
10.356 MeV	25.7(19) %	25.6(33) %
11.520 MeV	25.0(26) %	28.7(14) %
12.049 MeV	30.2(31) %	31.5(46) %

Table 2: States in ^{16}O with known 100% alpha branching ratios measured in this experiment. Here we compare a Monte Carlo simulation of SABRE's efficiency (i.e. branching ratios reported in [20] corrected for simulated geometric efficiency) with the measured yield in SABRE.

Comparing the measured 100% branching ratios of excited states in ^{16}O to the geometric efficiency of the array calculated in the simulation, given in Table 2, one finds that there is generally good agreement between the values. A deviation is observed for the 11.520-MeV state, which is difficult to extract as it is sitting on top of the 800-keV wide state at 11.6 MeV, which makes the background subtraction more difficult and may result in a measured branching ratio that is systematically larger than the expected value.

Additionally, a measurement of $^{27}\mathrm{Al}(^{3}\mathrm{He},t)^{27}\mathrm{Si}^{*}(p)^{26}\mathrm{Al}$ was performed to study proton branching ratios in ^{27}Si utilizing the thin-deadlayer detectors. During this measurement, energy thresholds in the detectors of roughly 190 keV were achieved when measuring protons from the decay of ^{27}Si [21].

5. Summary

A new silicon detector array for measuring charged-particle decay coincidences and branching ratios with the SE-SPS and its focal plane detector has been designed and implemented at Florida State University. It has a roughly 30% geometric efficiency for, e.g., the isotropic decay of the ^{16}O 12.049 MeV excited state and utilizes digital electronics, which have enabled higher rates and lower thresholds in the silicon detectors than other silicon arrays have yet achieved. The array's performance was tested against known branching ratios and compared with simulations, and meets the design goals. First experiments with SABRE include a study of ^{27}Si proton branching ratios for the ^{26}Al$(p,\gamma)^{27}$Si reaction in classical novae [21], a study of interference effects of two resonant states in ^{13}N, and a study of highly excited states in ^{9}B of importance to ^{7}Li abundances in Big Bang Nucleosynthesis calculations. SABRE is now a useful tool in both nuclear astrophysics and structure measurements with the SE-SPS at FSU.

Acknowledgements

Many thanks to the wonderful staff at Florida State University's John D. Fox Accelerator Laboratory and CAEN's support staff for all their help. This work was supported by the National Science Foundation Major Instrumentation Award No. PHY-1429189, FSU NSF grant No. PHY-1712953, and US Department Of Energy grant No. DE-SC0014231. E.C. Good was supported by the Department of Energy National Nuclear Security Administration Stewardship Science Graduate Fellowship program, which is provided under grant number DENA0003864.

References

[1] H. A. Enge, Nucl. Inst. Meth. 162 (1979) 161.

[2] C. Deibel, et al., Toward an experimentally determined $^{26}\mathrm{Al}(p,\gamma)^{27}\mathrm{Si}$ reaction rate in ONe novae, Phys. Rev. C 80 (2009) 035806.

[3] A. Chen, et al., Structure of ^{22}Mg and its implications for explosive nucleosynthesis, Phys. Rev. C 63 (2001) 065807.

[4] A. Parikh, et al., Mass measurements of ^{22}Mg and ^{26}Si via the $^{24}\mathrm{Mg}(p,t)^{22}\mathrm{Mg}$ and $^{28}\mathrm{Si}(p,t)^{26}\mathrm{Si}$ reactions, Phys. Rev. C 80 (2009) 035806.

[5] J. P. Schiffer, et al., Phys. Rev. Lett. 100 (2008) 112501.

[6] J. P. Schiffer, et al., Phys. Rev. Lett. 108 (2012) 022501.

[7] J. Spencer, H. Enge, Split-Pole Magnetic Spectrograph for Precision Nuclear Spectroscopy, Nuc. Instr. Meth. 49 (1967) 181–193.

[8] A. Parikh, Production of ^{26}Al in Oxygen-Neon-Magnesium Novae, Ph.D. thesis, Yale University (2006).

[9] D. Visser, Particle Decay Branching Ratios for States of Astrophysical Importance in ^{19}Ne, Ph.D. thesis, Yale University (2003).

[10] P. Adsley, R. Neveling, P. Papka, Z. Dyers, J. Brümmer, C. Diget, N. Hubbard, K. Li, A. Long, D. Marin-Lambarri, L. Pellegri, V. Pesudo, L. Pool, F. Smit, S. Triambak, CAKE: the coincidence array for k600 experiments, Journal of Instrumentation 12 (02) (2017) T02004–T02004. doi:10.1088/1748-0221/12/02/t02004.
URL https://doi.org/10.1088/1748-0221/12/02/t02004

[11] W. Bradfield-Smith, et al., On the behavior of ion implanted silicon strip detectors in high intensity low energy heavy ion beam experiments, Nuc. Instr. Meth. A 481 (2002) 183–187.

[12] CAEN S.p.A., WP2081: Digital Pulse Processing in Nuclear Physics, White paper, CAEN Electronic Instrumentation, rev. 3 (August 2011).

[13] CAEN S.p.A., UM2580: DPP-PSD: Digital Pulse Processing for Pulse Shape Discrimination, CAEN Electronic Instrumentation (September 2016).

[14] B. Davin, et al., LASSA: a large area silicon strip array for isotopic identification of charged particles, Nuc. Instr. Meth. A 473 (2001) 302–318.

[15] mesytec GmbH & Co. KG, Wernher-von-Braun- Str. 1, 85640 Putzbrunn, Germany, MDU 16 Data Sheet V1.0_02, accessed Feb. 26, 2020.

[16] V. T. Jordanov, G. F. Knoll, A. C. Huber, J. A. Pantazis, Digital techniques for real-time pulse shaping in radiation measurements, Nuclear Instruments and Methods in Physics Research Section A: Accelerators, Spectrometers, Detectors and Associated Equipment 353 (1-3) (1994) 261–264. doi:10.1016/0168-9002(94)91652-7.
URL https://linkinghub.elsevier.com/retrieve/pii/0168900294916527

[17] M. Corbo, Synchronization of CAEN Digitizers in Multiple Board Acquisition Systems 30.

[18] CAEN S.p.A., UM5960: Multiparametric DAQ Software for Physics Applications, Rev. 11, CAEN Electronic Instrumentation (April 2020).

[19] CAEN S.p.A., GD2827: How to make coinicidences with CAEN Digitizers, User guide, CAEN Electronic Instrumentation, rev. 3 (March 2017).

[20] D. Tilley, H. Weller, C. Cheves, Energy levels of light nuclei A = 16–17, Nuclear Physics A 564 (1) (1993) 1–183. doi:10.1016/0375-9474(93)90073-7.

[21] E. C. Good, A Study of $^{26}\mathrm{Al}(p,\gamma)^{27}\mathrm{Si}$ with the Silicon Array for Branching Ratio Experiments (SABRE), Ph.D. thesis, Louisiana State University (2020).